Journal of Materials Chemistry A

Accepted Manuscript

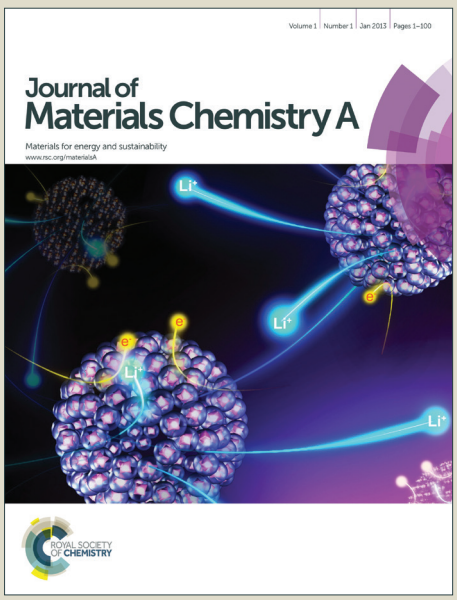

ROYAL SOCIETY OF CHEMISTRY

www.rsc.org/materialsA

Journal Name

RSCPublishing

COMMUNICATION

B_4C nanowires and carbon nanotubes composite as a novel bifunctional electrocatalyst for high energy lithium oxygen batteries

Cite this: DOI: 10.1039/xoxxoooooo

Received ooth January 2012,
Accepted ooth January 2012

DOI: 10.1039/xoxxoooooo

www.rsc.org/

Wen-Bin Luo, Shu-Lei Chou*, Jia-Zhao Wang, Hua-Kun Liu

B_4C nanowire as a novel bifunctional electrocatalyst was synthesized using carbon nanotubes as the template. Because of the highly efficient catalytic activity, together with the abundant catalytic sites in the B_4C nanowire and carbon nanotubes composite, this material exhibits great catalytic activity as an efficient bifunctional catalyst for the oxygen reduction and evolution reactions in lithium oxygen batteries. Excellent cycling performance under capacity limited mode is demonstrated, in which the terminal discharge voltage is higher than 2.2 V after 120 cycles at a current density of 0.4 mA cm^{-2}. This novel electrocatalyst is a promising bifunctional electrocatalyst for lithium oxygen batteries, with high energy density, favorable rechargeability, and high round-trip efficiency (76%).

Non-aqueous lithium oxygen battery was first described by Abraham and Jiang with high theoretical energy density (up to 2-3 kW kg^{-1}),[1] competing with that of any other conventional energy storage devices. It stores and converts energy between chemical energy and electrical energy via the electrochemical reaction of lithium and oxygen ($2Li^+ + O_2 + 2e^- = Li_2O_2$).[1-4] The deposition of Li_2O_2 at the positive electrode is a result of the oxygen reduction reaction (ORR, $O_2 + 2Li^+ + 2e^- \rightarrow Li_2O_2$), and the decomposition of Li_2O_2 during the charge process results from the oxygen evolution reaction (OER, $Li_2O_2 \rightarrow O_2 + 2Li^+ + 2e^-$). These two processes play significant role to determine the performance of Li-O_2 cells.[3,5,6] Therefore, it is necessary and important to develop a high efficient electrocatalyst to promote the ORR and OER for good cycling stability, and high energy efficiency. [2, 3, 7-12] Several types of electrocatalysts include carbon materials, [13-17] precious metals,[18-21] and transition metal oxides,[22-28] However, these materials all suffer in some way from low stability, high cost, or low efficiency, which limits their use in practical Li-O_2 battery electrodes. Therefore, it is vital to develop a novel electrocatalyst with high stability, low cost and high efficiency.

Boron carbide (B_4C), a lightweight refractory semiconductor, is the third hardest material known to man at room temperature. It has many unique properties, such as high resistance to chemical attack, high thermal stability, low density (2.5 g cm^{-3}), a small thermal expansion coefficient (5.73×10^{-6} K^{-1}), a high melting point (> 2400 ^oC), a high Seebeck coefficient, and a large neutron absorption cross-section.[29-34] To synthesize B_4C, a carbon source is essential, such as carbon black,[35,36] carbon nanotubes,[37-39] an organic carbon source, [40] or activated carbon.[41] Meanwhile, the application of carbon nanotubes (CNTs) in electrically conductive materials has attracted intense research interest because of their extraordinary thermal and mechanical stability, as well as the high electronic conductivity of CNTs.[42] To our best knowledge, there is no report using CNTs and B_4C composite for Li-O_2 batteries.

Herein, B_4C nanowires was synthesized using excess carbon nanotubes as the template and carbon source to react with boron powder to synthesize B_4C nanowires and carbon nanotubes composite, which can be used as a novel high efficient electrocatalyst in lithium oxygen batteries. In this composite, a carbon nanotube based network is used as a highly electronically conductive electrocatalyst support, and the stable B_4C nanowires act as a bifunctional electrocatalyst for both the ORR and the OER. The composite electrode exhibits excellent rechargeability and high round-trip efficiency as the air electrode in lithium oxygen batteries.

Journal Name

RSCPublishing

COMMUNICATION

B_4C nanowires and CNTs composite (sampled as BC in following) was characterized by the associated X-ray diffraction (XRD) and associated Raman spectroscopy, as shown in Fig. 1(a) and Fig. S1(a) in the Supporting Information. In Figure 1(a), aside from the peak of the CNTs at 26°, two peaks (marked with asterisks) at 2θ around 34.9° and 37.6° are observed in the final product, which correspond to the (21-31) and (11-2-1) crystalline planes of B_4C with a Norbide phase (JCSPDF: 35-0798). Meanwhile, the Raman spectrum of B_4C nanowire is in good agreement with a previous report.[43] Compared with pure B_4C nanowire and CNTs, Raman bands below 1200 cm^{-1} in the BC composite are detected, which can be assigned to the characteristic bonds of B_4C.[44,45] The field emission scanning electron microscope (FESEM) images in Fig. S1(b, c, d) also show large amounts of B_4C nanowire growing from the CNT aggregation with a diameter ranging from 40 to 100 nm and a length longer than 2 μm.

An atomic resolution analytical microscope (ARM) was used for scanning transmission electron microscopy (STEM) and elemental mapping analysis of B_4C nanowires in the composite, as shown in Figure 1(b, c, d). Energy dispersive X-ray spectroscopy (EDS) from the ARM, with results shown in the inset in Figure 1(b), reveals that the B and C elements display a uniform distribution and that the catalyst particle on or inside the nanowire tip is nickel. The STEM results also indicate typical crystal B_4C nanowires with a strongly crystalline texture grown from the CNTs aggregate. In Fig. 1(c), the structure of the crystal planes and the corresponding fast Fourier transform (FFT) of the individual nanowire [inset in Fig. 1(c)] exhibit a well-developed hexagonal single crystal with (11-20) and (-1-120) planes.[41,46] A highly resolved small area was also characterized by STEM together with FFT on the wall of the nanowire in Fig. 1(d). It can also be clearly demonstrated that the molecular packing along the relevant directions can be accurately determined at the atomic level. Meanwhile, the conclusion was obviously obtained from STEM that the nanowire growth direction is [-1-120] direction which crosses the (11-20) crystalline plane at an angle of ~30°. The growth direction was also observed by Dai.[46] In order to study the mechanism of B_4C nanowire formation in a catalytic synthesis process, we also performed a comparative experiment without using Ni (Fig. S2), and in this case, no B_4C nanowires were grown from the CNTs aggregation. Together with the EDS image (Fig. 1b) and the scanning electron microscope (SEM) image in Fig. S1(d), the conclusion can be drawn that the nickel catalyst particles on or inside the tip of each nanowire were spherical with a diameter distribution of 50 to 500 nm and that they played a catalytic role in growing such B_4C nanowires. To further verify the growth process, we carried out further tests by changing the annealing temperature and time. In Fig. S3(a, b), there are no B_4C nanowires formed when the temperature is lower than 1000 °C. When the temperature was increased to 1200 °C and maintained for 1 h, fewer and shorter B_4C nanowires were generated (Fig. S3(c)), and were twisted and turned in random directions. The B_4C nanowires were further grown and crystallized into a final structure by increasing time. Based on the results described and discussed above, the catalytic vapor-liquid-solid tip growth mechanism reported in previous research can explain the formation of the long single crystal B_4C nanowires, which can be schematically illustrated in Fig. 1(e).[47-50] In the initial stage, Ni salts were coated on the CNT surfaces or both ends, and the Ni was then deposited there. The deposited Ni provides catalytically active sites, absorbing boron vapor from the original solid boron raw material to form small Ni–B–C eutectic liquid droplets. When these droplets were oversaturated with boron and carbon, B_4C would start to nucleate and then grow from the droplets. After initial template formation, gaseous boron would continue to dissolve in the catalyst droplets, sustaining the B_4C growth. This explains the formation of the long single crystal B_4C nanowires.

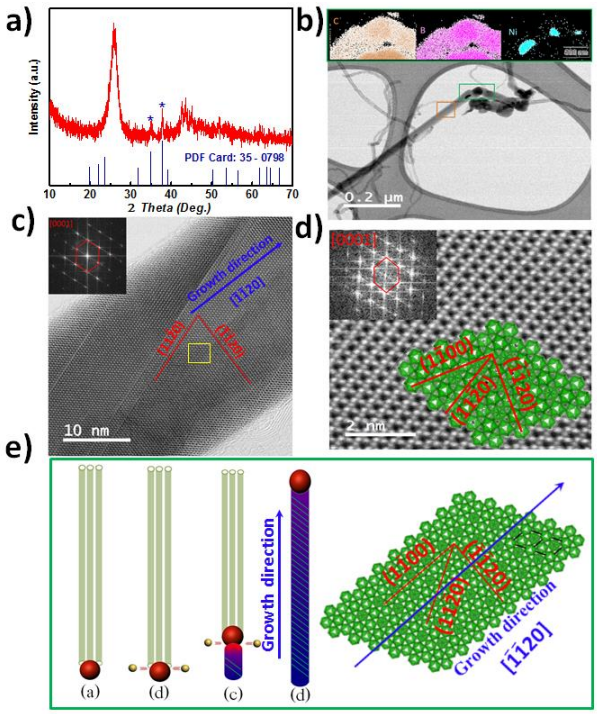

Figure 1 . a) X-ray diffraction pattern of BC composite; b) High resolution STEM image of the B_4C in the BC composite and EDS mapping for C, B, and Ni elements(marked green square frame for EDS scan area; marked yellow square frame for(c)); c) STEM image of a B_4C nanowire in the BC composite (inset: corresponding FFT pattern; marked yellow square frame for(d)); d) STEM image of small area on the wall of B_4C nanowire, with the inset showing the corresponding FFT pattern; e) (left) schematic diagram of the B_4C nanowire formation mechanism (light green cylinders: CNTs, red balls: nickel catalyst, yellow balls: boron gas, blue cylinders: B_4C); the diagrams of the B_4C crystal structure on the right of (e) and inset of (d) come from VESTA software.[40]

The rotating disk electrode (RDE) technique was used to investigate the ORR activities of three samples in O_2-saturated 0.1 M KOH electrolyte at a scan rate of 10 mV s^{-1}, including high-quality commercial Pt/C (20 wt% Pt on Vulcan XC-72), CNTs/Ni composite (sampled as CN in following), and BC composites. As shown in the RDE curves in Fig 2(a) and Fig.S4, compared with CN composite and commercial Pt/C, BC composite showed an enhanced ORR performance with positive onset potential and large current density, which correspond to excellent ORR catalyst activity. Furthermore, RDE curves of Pt/C, CN composite, and BC composites at various rotation speeds were measured to determine their ORR kinetic performance (details in the Supporting Information). The corresponding Koutecky-Levich (K–L) plots (J^{-1} vs. $\omega^{-1/2}$) at various electrode potentials exhibited good linearity (Fig.S4). The linearity and parallelism of the K–L plots suggest first-order reaction kinetics toward the concentration of dissolved oxygen and similar electron transfer numbers for the ORR at different potentials. The BC composite favors a nearly 4 electron oxygen reduction reaction process, similar to the ORR catalyzed by a high-quality commercial Pt/C catalyst (n = 4.0), but more than that of CN composite (3.2 - 3.5). Owing to the steep gradient (or Tafel slope) of the polarization curves during ORR, the ORR kinetics of BC composite is definitely superior to that of CN composite. BC composite shows the excellent similar ORR kinetic Tafel slope (~ 63 mV dec^{-1}) as the high-quality commercial Pt/C catalyst (~59 mV dec^{-1}). Moreover, the OER activities of the electrocatalyst are shown in Fig. 2(c). The BC composite also shows much more excellent catalytic activity towards the OER than high-quality commercial Pt/C and CNTs@Ni. In corresponding comparison OER kinetic current as shown in Fig. 2(d), the slopes of the curves indicates different kinetic OER activities. Excellent OER activity of the BC composite was also found from the smaller Tafel slope of 70 mV dec^{-1} than that measured with Pt/C (123 mV dec^{-1}). Therefore, BC composite can act as a bifunctional catalyst, which shows excellent catalytic activity with smaller over-potential for both the ORR and OER than high-quality commercial Pt/C. To investigate the ORR and OER processes in non-aqueous electrolyte, steady-state cyclic voltammograms (CVs) were collected under oxygen saturated conditions with a scan rate of 10 mV s^{-1} at 900 rpm (Figure 2e). Compared with the CN composite, the BC composite shows obvious smaller over-potential in O_2-saturated electrolyte, which indicate that BC features bifunctional catalyst performance in the anodic and cathodic scan processes.

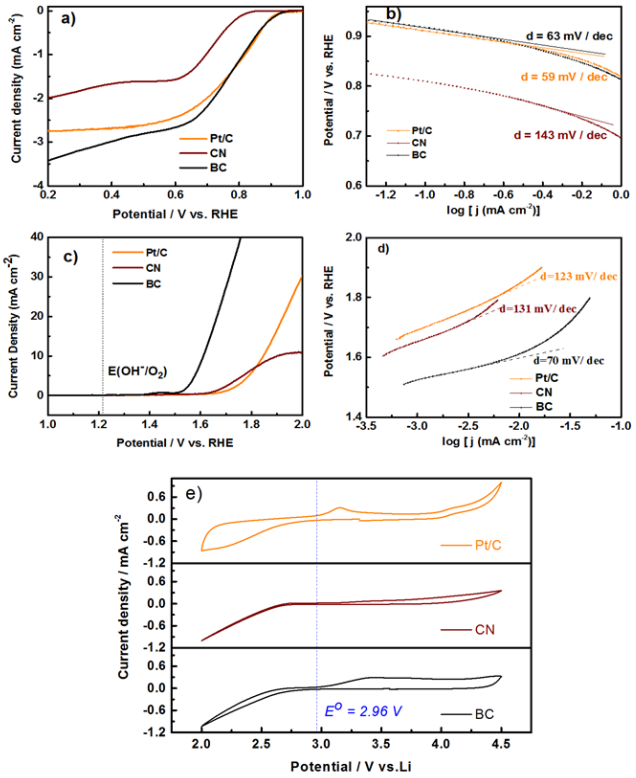

Figure 2. (a) Comparison of RDE curves of commercial Pt/C (20 wt% Pt on Vulcan XC-72), CN and BC composite in O_2-saturated 0.1 M KOH solution with 900 rpm rotation speed and a sweep rate of 10 mV s^{-1}; (b) Tafel plots showing the kinetic current density of commercial Pt/C, CN and BC composite as a function of potential, based on data from (a); (c) Oxygen evolution reaction currents of commercial Pt/C, CN and BC composite in O_2-saturated 0.1 M KOH solution with 900 rpm rotation speed and a sweep rate of 10 mV s^{-1}; (d) Tafel plots showing the kinetic current density of commercial Pt/C, CN and BC composite as a function of potential, based on data from (c); (e) CV curves acquired at 10 mV s^{-1} in O_2 saturated $LiCF_3SO_3$ in TEGDME (molar ratio = 1:4) electrolyte with 900 rpm rotation speed.

The electrochemical properties of samples were then examined in a lithium oxygen cell without adding conductive carbon black. The specific capacities were calculated based on the total composite mass in the air cathodes. The BC composite exhibits a higher discharge voltage plateau and a lower charge potential that is vital for electrochemical energy storage devices, as well as delivering nearly 16000 mAh g^{-1} at 0.2 mA cm^{-2} current density (Fig. S5). Furthermore, the discharge voltage of BC composite, 2.73 V, is higher than that of reported electrocatalysts.[15,18,23,24] The BC composite also shows higher discharge/charge capacity of about 11000/10000 and 9300/8000 mAh g^{-1} at the different current densities of 0.4 and 0.6 mA cm^{-2}, respectively. This may result from the enormous density of sites for reaction product deposition provided by the porous CNTs' aggregated structure and the high electrocatalyst efficiency of BC composite. Following the recently widely used capacity-limited cycling method,[16] Fig. 3(a) shows a comparison of first discharge/charge voltage profiles of the pure CNTs mixed with additional nickel (CN) after the same annealing

process and BC composite at the current density of 0.4 mA cm^{-2}. The discharge potential plateau of BC composite is 130 mV higher than that of CN composite, and the charge potential plateau of BC composite is 720 mV lower than that of CN composite, rendering a higher round-trip efficiency of 76%. The higher round-trip efficiency could be largely attributed to the high efficiency electrocatalyst role of B_4C during the reaction. BC composite not only shows a higher ORR potential and lower OER potential [Fig. S6(a)], but also presents excellent cycling performance. In Fig. 3(b), the BC composite shows a stable cycling performance, and the voltage obtained at the discharge terminal is higher than 2.2 V for 120 cycles when the cut-off capacity is 1000 mAh g^{-1}. The BC composite also exhibits a lower overpotential (at 500 mAh g^{-1} position) than CN composite during the 120 cycles. Meanwhile, with the cut-off capacity increased to 2000 and 3000 mAh g^{-1}, as shown in [Fig. S6(b-e)], the BC composite also exhibits stable cycling performance, and the voltage obtained at the discharge terminal is higher than 2.2 V for 49 and 20 cycles, respectively. Therefore, the BC composite exhibits excellent electrochemical performance towards both the formation and the decomposition of discharge products (Li_2O_2), which might be attributed to substantial reaction sites for the reaction and deposition of nanocrystalline products originating from the macroporous electrode structure, while the high round-trip and cycling performance result from the efficient synergistic effect of the high electrocatalyst reactions toward the ORR and OER processes from B_4C, which are vital for electrochemical energy storage devices.

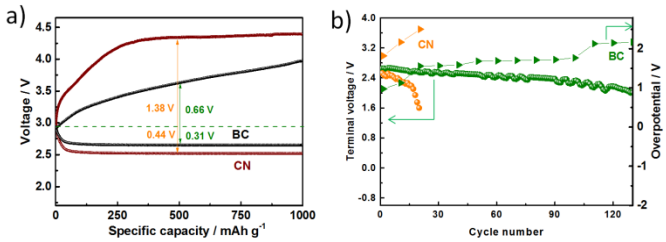

Figure 3. a) Comparison of first discharge/charge voltage profiles of CN and BC composite at 0.4 mA cm^{-2} with a fixed capacity of 1000 mAh g-1; b) cycling performance at 0.4 mA cm^{-2} with a fixed capacity of 1000 mAh g^{-1};

To further elucidate the BC composite reaction mechanism, the phases and morphologies of reaction products at discharge and recharge stages are shown in Figure 4. According to the XRD results, there is a clear evidence of crystalline Li_2O_2 formation at the end of discharge. When recharging follows, the discharge product on the electrode, Li_2O_2, cannot be detected by XRD in Fig. 4(a). This is consistent with the results obtained by other groups.[51-59] Therefore, the BC composite shows excellent rechargeability performance during discharge/charge cycling. Meanwhile, understanding the nucleation process of different morphologies of Li_2O_2 and clearly related influential factors could provide valuable insight into the mechanism of the reaction as well as into the design of a proper catalyst and electrode structure for practical devices. So, the corresponding morphologies of the reaction product after the first full discharge, crystalline Li_2O_2, were observed using FESEM. In the discharge process, a large amount of dendritic Li_2O_2 nanorod in the range of 50 nm is regularly deposited on the cathode, the great majority of which nucleates on the walls of the B_4C nanowire. The deposition reaction product of Li_2O_2 on the surface of CN electrode during the ORR process is very large toroid-like particles up to 1 μm in size as shown in Fig. S7, which is similar to the previous report on the morphology of Li_2O_2.[11,60,61] It is clear that the different morphology of electrocatalysts can also influence the morphology of the Li_2O_2 reaction product. Consequently, the morphology and size of the reaction products may result in different electrochemical performance. In the following charge process, reaction products, mainly Li_2O_2, were decomposed, and the B_4C nanowires appear again in the corresponding image in Fig. 4(c), which is also in agreement with the XRD results.

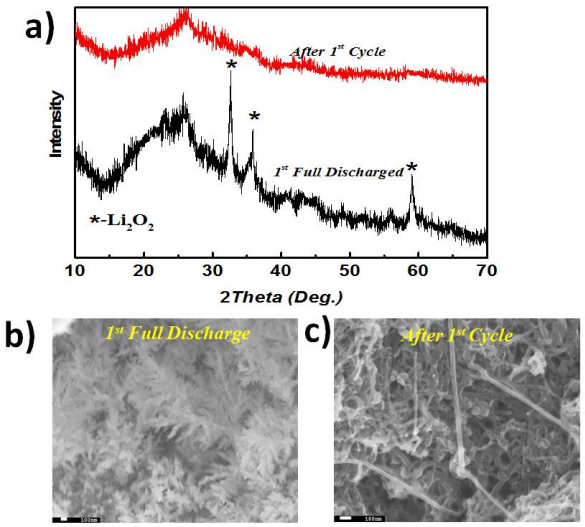

Figure 4. a) XRD patterns and b, c) FESEM images of the composite after 1st full discharge and after 1st cycle.

Conclusions

In summary, B_4C nanowire was synthesized by a simple reaction between CNTs and boron nanopowders using nickel as the catalyst at high temperature. As-prepared BC composite was used as cathode material in lithium oxygen battery. B_4C nanowires can act as an efficient bifunctional electrocatalyst and promote the formation of dendritic type of Li_2O_2. The electrochemical results on the BC composite show nearly 16000 mAh g^{-1} capacity above 2.5 V at 0.2 mA cm^{-2} current density and a 2.73 V discharge voltage plateau. Excellent cycling performance is also demonstrated, in which the terminal voltage is higher than 2.2 V after 120 cycles at 0.4 mA cm^{-2}, with 1000 mAh g^{-1} capacity limitation. All of the good performance is attributed to the excellent catalytic performance of the enormous B_4C nanowires towards the ORR and OER reactions in the composite. Therefore, this BC composite is a promising bifunctional electrocatalyst for lithium oxygen batteries, with high energy density, favorable rechargeability, and high round-trip performance.

Acknowledgements

The authors are grateful for funding from the Australian Research Council (ARC) under a Linkage Project (LP120200432) and a Discovery Project (DP140100401). The authors also thank Dr. T. Silver for critical reading of the manuscript, and also acknowledge the use of the facilities in the UOW Electron Microscopy Center, with particular thanks to Dr. Gilberto Casillas-Garcia.

Notes and references

Institute for Superconducting and Electronic Materials, University of Wollongong, Wollongong, NSW 2522 Australia

† Footnotes should appear here. These might include comments relevant to but not central to the matter under discussion, limited experimental and spectral data, and crystallographic data.
Electronic Supplementary Information (ESI) available: [including HFSEM images, Raman results, Rotating disk electrode performance, and electrochemical data]. See DOI: 10.1039/c000000x/

1 K. M. Abraham, Z. Jiang, *J Electrochem Soc* 1996, **143**, 1.
2 P. G. Bruce, S. A. Freunberger, L. J. Hardwick, J. M. Tarascon, *Nat Mater* 2012, **11**, 19.
3 J. Christensen, P. Albertus, R. S. Sanchez-Carrera, T. Lohmann, B. Kozinsky, R. Liedtke, J. Ahmed, A. Kojic, *J Electrochem Soc* 2012, **159**, R1.
4 M. Park, H. Sun, H. Lee, J. Lee, J. Cho, *Adv Energy Mater* 2012, **2**, 780.
5 R. Black, B. Adams, L. F. Nazar, *Adv Energy Mater* 2012, **2**, 801.
6 S. Nakanishi, F. Mizuno, K. Nobuhara, T. Abe, H. Iba, *Carbon*. 2012, **50**, 4794.
7. H. Kim, H. D. Lim, J. Kim and K. Kang, *J Mater Chem A*, 2014, **2**, 33.
8 Y. Y. Shao, S. Park, J. Xiao, J. G. Zhang, Y. Wang, J. Liu, *Acs Catal* 2012, **2**, 844.
9 S. H. Oh, L. F. Nazar, *Adv Energy Mater* 2012, **2**, 903.
10 Y. Y. Shao, F. Ding, J. Xiao, J. Zhang, W. Xu, S. Park, J. G. Zhang, Y. Wang, J. Liu, *Adv Funct Mate*r 2013, **23**, 987.
11 Y. C. Lu, B. M. Gallant, D. G. Kwabi, J. R. Harding, R. R. Mitchell, M. S. Whittingham, Y. Shao-Horn, *Energ Environ Sci* 2013, **6**, 750.
12 R. Black, S. H. Oh, J. H. Lee, T. Yim, B. Adams, L. F. Nazar, *J Am Chem Soc* 2012, **134**, 2902.
13 H. D. Lim, K. Y. Park, H. Song, E. Y. Jang, H. Gwon, J. Kim, Y. H. Kim, M. D. Lima, R. O. Robles, X. Lepro, R. H. Baughman, K. Kang, *Adv Mater* 2013, **25**, 1348;
14 Y. G. Wang, H. S. Zhou, Energ Environ Sci 2011, **4**, 1704.
15 J. Xiao, D. H. Mei, X. L. Li, W. Xu, D. Y. Wang, G. L. Graff, W. D. Bennett, Z. M. Nie, L. V. Saraf, I. A. Aksay, J. Liu, J. G. Zhang, *Nano Lett* 2011, **11**, 5071.
16 H. G. Jung, J. Hassoun, J. B. Park, Y. K. Sun, B. Scrosati, *Nat Chem* 2012, **4**, 579.
17 W.B. Luo, S.L. Chou, J.Z. Wang, Y.C. Zhai, H.K. Liu, *Small* 2015,**10**,1002.
18 Z. L. Jian, P. Liu, F. J. Li, P. He, X. W. Guo, M. W. Chen, H. S. Zhou, *Angew Chem Int Edit* 2014, **53**, 442.
19 J. J. Xu, D. Xu, Z. L. Wang, H. G. Wang, L. L. Zhang, X. B. Zhang, *Angew Chem Int Edit* 2013, **52**, 3887.
20 Y. C. Lu, Z. C. Xu, H. A. Gasteiger, S. Chen, K. Hamad-Schifferli, Y. Shao-Horn, *J Am Chem Soc* 2010, **132**, 12170.
21 Z. Q. Peng, S. A. Freunberger, Y. H. Chen, P. G. Bruce, Science 2012, **337**, 563.
22 D. O. Atienza, T. C. Allison, Y. Y. J. Tong, *J Phys Chem C* 2012, **116**, 26480.
23 A. Debart, A. J. Paterson, J. Bao, P. G. Bruce, *Angew Chem Int Edit* 2008, **47**, 4521.
24 L. X. Zhang, S. L. Zhang, K. J. Zhang, G. J. Xu, X. He, S. M. Dong, Z. H. Liu, C. S. Huang, L. Gu, G. L. Cui, *Chem Commun* 2013, **49**, 3540.
25 H. D. Lim, H. Gwon, H. Kim, S. W. Kim, T. Yoon, J. W. Choi, S. M. Oh, K. Kang, *Electrochim Acta* 2013, **90**, 63.
26 M. S. Park, J. H. Kim, K. J. Kim, G. Jeong, Y. J. Kim, *J Nanosci Nanotechno* 2013, **13**, 3611;
27 H. W. Park, D. U. Lee, L. F. Nazar, Z. W. Chen, *J Electrochem Soc* 2013, **160**, A344.
28 J. Sun, J. Zhang, M. Zhang, M. Antonietti, X. Fu, X. Wang, *Nat Commun* 2012, **3**, 1139.
29 K. A. Schwetz, L. S. Sigl, L. Pfau, *J Solid State Chem* 1997, **133**, 68.
30 C. Chen, D. W. He, Z. L. Kou, F. Peng, L. Yao, R. C. Yu, Y. Bi, *Adv Mater* 2007, **19**, 4288.
31 M. Karaman, N. A. Sezgi, H. O. Ozbelge, *Aiche J* 2009, **55**, 2914.
32 E. Kroke, K. W. Volger, A. Klonczynski, R. Riedel, *Angew Chem Int Edit* 2001, **40**, 1698.
33 R. Ruh, M. Kearns, A. Zangvil, Y. R. Xu, *J Am Ceram Soc* 1992, **75**, 864.
34 E. M. Sharifi, F. Karimzadeh, M. H. Enayati, *Adv Powder Technol* 2011, **22**, 354.
35 R. Ma, Y. Bando, *Chem Mater* 2002, **14**, 4403.
36 R. Z. Ma, Y. Bando, *Chem Phys Lett* 2002, **364**, 314.
37 W. Q. Han, S. S. Fan, Q. Q. Li, W. J. Liang, B. L. Gu, D. P. Yu, *Chem Phys Lett* 1997, **265**, 374.

38 J. Q. Wei, B. Jiang, Y. H. Li, C. L. Xu, D. H. Wu, B. Q. Wei, *J Mater Chem* 2002, **12**, 3121.
39 W. Q. Han, S. S. Fan, Q. Q. Li, W. J. Liang, B. L. Gu, D. P. Yu, *Chem Phys Lett* 1997, **265**, 374.
40 X. Y. Tao, L. X. Dong, X. N. Wang, W. K. Zhang, B. J. Nelson, X. D. Li, *Adv Mater* 2010, **22**, 2055.
41 W. Q. Han, *Appl Phys Lett* 2006, **88**,242505.
42 C. Liu, F. Li, L. P. Ma, H. M. Cheng, *Adv Mater* 2010, **22**, E28.
43 K. M. Reddy, P. Liu, A. Hirata, T. Fujita, M. W. Chen, *Nat Commun* 2013, **4**,17.
44 H. Werheit, T. Au, R. Schmechel, S. O. Shalamberidze, G. I. Kalandadze, A. M. Eristavi, *J Solid State Chem* 2000, **154**, 79.
45 R. Lazzari, N. Vast, J. M. Besson, S. Baroni, A. Dal Corso, P*hys Rev Lett* 1999, **83**, 3230.
46 H. J. Dai, E. W. Wong, Y. Z. Lu, S. S. Fan, C. M. Lieber, *Nature* 1995, **375**, 769.
47 J. T. Huang, Z. H. Huang, S. Yi, Y. G. Liu, M. H. Fang, S. W. Zhang, *Sci Rep-Uk* 2013, **3**,3504.
48 J. Huang, S. Zhang, Z. Huang, Y. g. Liu, M. Fang, *Crystengcomm* 2013, **15**, 785.
49 C. C. Tang, Y. Bando, T. Sato, K. Kurashima, *J Mater Chem* 2002, **12**, 1910.
50 L. M. White, M. H. Kim, J. P. Zhang, S. Kraemer, C. T. Yavuz, M. Moskovits, A. M. Wodtke, G. D. Stucky, *J Mater Chem A* 2013, **1**, 6091.
51 Y. C. Lu, H. A. Gasteiger, E. Crumlin, R. McGuire, Y. Shao-Horn, *J Electrochem Soc* 2010, **157**, A1016.
52 J. L. Shui, J. S. Okasinski, D. Zhao, J. D. Almer, D. J. Liu, *Chemsuschem* 2012, **5**, 2421.
53 K. R. Ryan, L. Trahey, J. S. Okasinski, A. K. Burrell, B. J. Ingram, *J Mater Chem A* 2013, **1**, 6915.
54 Y. M. Cui, Z. Y. Wen, Y. Liu, *Energ Environ Sci* 2011, **4**, 4727.
55 G. Wu, N. H. Mack, W. Gao, S. G. Ma, R. Q. Zhong, J. T. Han, J. K. Baldwin, P. Zelenay, *Acs Nano* 2012, **6**, 9764.
56 E. Yoo, H. S. Zhou, *Acs Nano* 2011, **5**, 3020.
57 F. Y. Cheng, J. A. Shen, B. Peng, Y. D. Pan, Z. L. Tao, J. Chen, *Nat Chem* 2011, **3**, 79.
58 H. G. Jung, Y. S. Jeong, J. B. Park, Y. K. Sun, B. Scrosati, Y. J. Lee, *Acs Nano* 2013, **7**, 3532.
59 J. Lu, Y. Lei, K. C. Lau, X. Y. Luo, P. Du, J. G. Wen, R. S. Assary, U. Das, D. J. Miller, J. W. Elam, H. M. Albishri, D. Abd El-Hady, Y. K. Sun, L. A. Curtiss, K. Amine, *Nat Commun* 2013, **4**,2383.
60 R. R. Mitchell, B. M. Gallant, C. V. Thompson, Y. Shao-Horn, *Energ Environ Sci* 2011, **4**, 2952.
61 S. H. Oh, R. Black, E. Pomerantseva, J. H. Lee, L. F. Nazar, Nat *Chem 2012*, **4**, 1004.

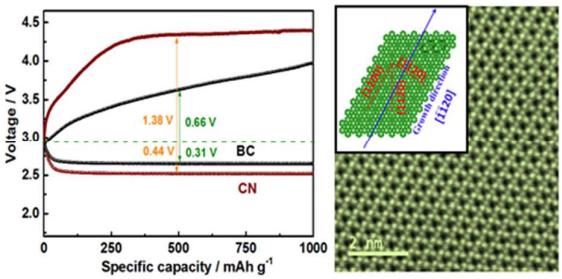

B_4C nanowire, a novel bifunctional electrocatalyst, is used as electrocatalyst for Li-O_2 batteries, with favourable rechargeability, and high round-trip efficiency.